SEISMIC DATA RECONSTRUCTION VIA COMPLEX SHEARLET TRANSFORM AND BLOCK COORDINATE RELAXATION

JICHENG LIU, YA GU and YONGXIN CHOU

School of Electrical & Automatic Engineering, Changshu Institute of Technology. Changshu 215500, P.R. China. jcliu@cslg.edu.cn

(Received May 1, 2018; revised version accepted February 12, 2019)

ABSTRACT

Liu, J., Gu, Y. and Chou, Y.X., 2019. Seismic data reconstruction via complex shearlet transform and block coordinate relaxation. *Journal of Seismic Exploration*, 28: 307-332.

Due to practical and economic limitations, real seismic data is not densely sampled in all coordinates, which will affect the subsequent seismic data processing steps, such as migration, surface-related multiple elimination and inversion. Therefore, it is necessary to reconstruct the incomplete seismic data. This paper explains the application of the complex shearlet transform to seismic data reconstruction. With a L_1 constraint and the Block Coordinate Relaxation (BCR) method, performance of the complex shearlet-based, real shearlet-based and well-accepted curvelet-based reconstruction are compared in terms of recovered *f-k* spectrum and signal to noise ratio (SNR). We also discuss the shift invariance of the complex shearlet transform and compare the performances of the BCR and the widely used Projection Onto Convex Sets (POCS) method. The numerical experiments on synthetic and real data with different under-sampling rates demonstrate the validity of the proposed method, especially for the case of large amounts of traces missing.

KEY WORDS: seismic data reconstruction, complex shearlet transform, curvelet transform, block coordinate relaxation.

INTRODUCTION

In the process of field seismic data acquisition, the geophones are regularly arranged and record the seismic signal generated by the sources. In order to avoid information loss, the Nyquist criterion should be fulfilled for the spatial sampling. But influenced by the acquisition environment, such as the presence of obstacles, forbidden areas, dead traces, and, most importantly, economic considerations, seismic data is always irregularly and incompletely sampled along spatial coordinates, which will introduce spatial aliasing. As a

0963-0651/19/$5.00

result, the sparse seismic data can not satisfy the subsequent processing techniques such as velocity analysis, surface-related multiple elimination and migration. So the reconstruction of seismic data to a user-defined denser grid is a very important problem in the seismic community as the quality of reconstruction will impact the subsequent seismic processing steps. Furthermore, using an appropriate reconstruction method can reduce the acquisition cost and improve the acquisition efficiency.

The reconstruction methods of irregular seismic data are commonly divided into three categories: First, there are methods based on the wave equation (Ronen, 1987; Chemingui and Biondi, 2002; Fomel, 2003), which combines the wave equation and a DMO (Dip Moveout) or an AMO (Azimuth Moveout) operator to reconstruct seismic data. However, the intensive computation of the wave equation and the difficulty of obtaining an accurate subsurface velocity model limit the application of such methods; second, the prediction filter-based methods (Spitz, 1991; Guo et al., 1996; Zhou, 1997; Porsani, 1999; Naghizadeh and Sacchi, 2007,2009) can improve the computation efficiency and reconstruction performance and are widely used in practice; third, the reconstruction methods based on mathematical transform and signal analysis (Herrmann and Hennenfent, 2008; Gao et al., 2010; Naghizadeh and Innanen, 2011; Yang et al., 2012; Wang et al., 2014; Wang et al., 2015) utilize the signal characteristics in the transform domain to reconstruct seismic data, such as Fourier transform (Abma and Kabir, 2006), Radon transform (Kabir and Verschuur, 1995), curvelet transform (Herrmann and Hennenfent, 2008, Cao et al., 2011, 2012; Cao and Wang, 2014, 2015c; Cao et al., 2015a, Cao and Zhao, 2015b) and Seislet transform (Liu et al., 2017). In addition, the rank reduction method (Gao et al., 2013; Ma, 2013) has also aroused interest.

According to the Compressed Sensing (CS) theory, the irregularly down-sampled seismic data can be effectively reconstructed by a sparsity-promoting L_1-norm convex optimization approach, which indicates that the measured incomplete seismic data can be used to reconstruct the missing seismic data with high precision. Using the fact that the curvelet transform can sparsely represent linearly shaped features, Herrmann et al. (2008) applied the sparsity-promoting L_1-norm minimization of curvelet coefficients to reconstruct seismic data.

The shearlet transform (Guo et al., 2006) is a new kind of multi-dimensional function approximation method. Compared to the curvelet transform, the shearlet transform conforms a tight frame theory and has a strict mathematical derivation, its directional filters have no pseudo Gibbs' phenomena arising from sampling. Compared to the curvelet transform, the discrete version of the shearlet transform is easy to implement and its complexity regarding the calculation is greatly reduced. As a result, the shearlet transform was quickly applied to various fields since it was proposed (Kutyniok and Labate, 2009; Pejoski et al., 2015; Pein et al., 2016).

The shearlet transform has very good localization features and its decomposition algorithm is similar to that of the wavelet transform (Kutyniok and Labate,2012) because it can be deduced through the tight frame system of multi-scale analysis. The characteristic of the shearlet transform makes it very suitable for processes like image edge detection and de-noising (Easley et al., 2008; Sheng et al., 2009; Wang, 2010; Genzel and Kutyniok, 2014; Kong and Peng, 2015). Feng et al. (2016) reconstructed 2D seismic data based on the shearlet transform using a POCS algorithm, where the NMO correction prior to reconstruction is adopted to strengthen the sparsity of the seismic data. Zhang et al. (2017) combined the shearlet transform with an Orthogonal Matching Pursuit (OMP) algorithm to reconstruct the 2D seismic data, and they also compared the reconstruction performance of different sparse transforms such as Fourier transform, discrete cosine transform, wavelet transform and curvelet transform. Liu et al. (2018) proposed the method based on the shearlet transform and the Projection Onto Convex Sets (POCS) with a L_0-norm constraint to interpolate irregularly sampled 2D and 3D seismic data.

Decomposition based on the shearlet transform has provided an optimally sparse approximation of a certain class of natural images, but the shearlet transform has no shift-invariant characteristics because of utilizing the Laplace pyramid structure in the multi-scale analysis. Kutyniok and Labate (2007) proposed to replace the Laplace pyramid with a non-down-sampled Laplace pyramid, which makes the shearlet transform having a shift-invariant characteristic. However, this method increases the redundancy of the non-down-sampling based shearlet transform greatly and it leads to a very slow computation speed. Lim et al. (2010) constructed the non-separable compactly supported shearlet generators, which can better approximate the classical band-limited generators whose Fourier transforms have wedge-like support. Many experimental results demonstrated that the method outperforms the other algorithms in most tasks when concerning speed (Kutyniok and Petersen, 2015; Kutyniok et al., 2016).

Just like the wavelet case, a function $\psi \in L^2(R^2)$ is said to be an admissible shearlet if it satisfies

$$\int_{R^2} \frac{|\hat{\psi}(\omega_1, \omega_2)|}{\omega_1^{\,2}} d\omega_1 d\omega_2 < \infty \quad ,$$

where $L^2(\cdot)$ is a square integrable space, $\hat{\psi}$ denotes the two-dimensional Fourier transform of ψ, w_1 and w_2 are the frequency components of the horizontal and vertical direction respectively. Therefore, the shearlet admissibility condition is only dependent on the absolute value of the Fourier transform of a candidate function. If the Fourier transform of a function is compactly supported away from the origin, the function is an admissible shearlet. In addition, the scaling or shearing of a shearlet generator can be characterized by the respective changes in the frequency plane, so similar to the Fourier transform with shift invariance in the

magnitude response, the complex shearlet transform, which has the characteristic of shift invariance, can be constructed utilizing the algorithm proposed by Kutyniok et al. (2016). Reisenhofer et al. (2016) presented a novel edge and ridge (line) detection algorithm that is based on the complex shearlet transform, and they used the method to extract flame fronts.

The POCS algorithm has been widely used in image and irregular seismic data reconstruction because of its high efficiency and reconstruction performance (Ozkan et al., 1994; Patti et al., 1997; Abma and Kabir, 2006; Yang et al., 2012; Wang et al., 2015, 2016; Wang, 2016). The algorithm requires some closed convex constrainted sets defined in a vector space, then any initial estimation is projected to these constrainted sets and a high resolution image can be estimated. In this paper, we use the Block Coordinate Relaxation (BCR) method as a sparse promoting strategy. BCR was proposed to solve the basis pursuit based de-noising problem, which has the advantages of simplicity and rapid convergence speed (Bruce et al., 1998). Based on the complex shearlet transform, we compare the performance of POCS and BCR method to reconstruct seismic data.

The main contributions of the paper are as follows: first, we propose a method based the complex shearlet transform and BCR to reconstruct seismic data. The numerical experiments demonstrate that the method performs better than the real shearlet transform and the well-accepted curvelet transform methods. Second, we compare the performance of the complex shearlet transform and the real shearlet transform to reconstruct seismic data. Third, we also discuss the performance of the POCS and BCR algorithms. From the numerical results, it can be seen that the BCR algorithm has a more rapid convergence speed than the POCS algorithm.

The paper is organized as follows. In the first section, we introduce the complex shearlet transform and the BCR method. Then the procedure of reconstructing 2D seismic data, which is based on the complex shearlet transform using the BCR algorithm, is illustrated. The Method section demonstrates the tests on 2D synthetic and real data with different under-sampled rates, which proves the validity of the proposed method. In the Numerical Examples section, we discuss the advantage of the complex shearlet transform compared to the real shearlet transform and also compare the performance of the POCS and BCR algorithms. The last section concludes the paper.

METHOD

The Complex shearlet transform

The wavelet transform has only point singularities because of its isotropy, which makes it have no ability to extract directional information and can not deliver highly sparse approximations of 2D signals. Therefore, many different transforms are proposed to extract the geometry information from

2D or higher dimensional data sets. Among these transforms, the curvelet transform works better for events that can be well approximated by local plane waves and has been widely applied in seismic data reconstruction.

The shearlet transform (Guo et al., 2006) combines the composite wavelet transform with multi-scale analysis and constructs an optimally sparse representation of a multi-dimensional signal. The shearlets have more sensitive directionality and provide a more sparse representation compared to the curvelets and the contourlets (Candès and Donoho, 2004; Minh and Vetterli, 2005). Because the shearlet transform adopts shearing operators which has consistency with the digital lattice, the continuum and digital realm of shearlet transform was treated uniformly in the sense of the continuum theory allowing a faithful implementation (Kutyniok et al. 2012).

A continuous shearlet system can be defined as follow:

$$\{\boldsymbol{\psi}_{a,s,\mathbf{t}}(\mathbf{x}) : a > 0, s \in \mathbf{R}, \mathbf{t} \in \mathbf{R}^2, \mathbf{x} \in \mathbf{R}^2\},$$

where

$$\boldsymbol{\psi}_{a,s,\mathbf{t}}(\mathbf{x}) = a^{3/4}\boldsymbol{\psi}(\mathbf{B}_s\mathbf{A}_a(\mathbf{x}-\mathbf{t}))$$

is the shearlet, $\boldsymbol{\psi}$ is the mother wavelet, $\mathbf{B}_s = \begin{pmatrix} 1 & s \\ 0 & 1 \end{pmatrix}$ is the shearing matrix, $\mathbf{A}_a = \begin{pmatrix} a & 0 \\ 0 & \sqrt{a} \end{pmatrix}$ is the parabolic scale matrix, **x** is a spatial location, **t** is the spatial translation parameter. Let $a = 2^j$, $s = l$, $\mathbf{t}=\mathbf{k}$ $j, l \in \mathbb{Z}, \mathbf{k} \in \mathbb{Z}^2$, then $\mathbf{A}_{2^j} = \begin{pmatrix} 2^j & 0 \\ 0 & 2^{j/2} \end{pmatrix}, \mathbf{B}_l = \begin{pmatrix} 1 & l \\ 0 & 1 \end{pmatrix}$, the discrete shearlet is

$$\boldsymbol{\psi}_{2^j,l,\mathbf{k}}(\mathbf{x}) = 2^{\frac{3j}{4}}\boldsymbol{\psi}(\mathbf{B}_l\mathbf{A}_{2^j}\mathbf{x}-\mathbf{k}).$$

In order to get a better directional selectivity both from the horizontal and vertical point of view, the cone-adapted shearlets are usually used. The cone-adapted shearlet system is defined as (Kutyniok et al., 2016)

$$S(\boldsymbol{\varphi}, \boldsymbol{\psi}, \tilde{\boldsymbol{\psi}}; \mathbf{c}) = \Phi(\boldsymbol{\varphi}, c_1) \cup \Psi(\boldsymbol{\psi}, \mathbf{c}) \cup \tilde{\Psi}(\tilde{\boldsymbol{\psi}}, \mathbf{c}),\ \boldsymbol{\varphi}, \boldsymbol{\psi}, \tilde{\boldsymbol{\psi}} \in L^2(\mathbf{R}^2), \mathbf{c} = (c_1, c_2) \in \mathbb{R}_+^2 \quad (1)$$

where

$$\Phi(\boldsymbol{\varphi}, c_1)=\{\boldsymbol{\varphi}_m=\boldsymbol{\varphi}(\mathbf{x}-c_1\mathbf{k}), \mathbf{k}\in\mathbb{Z}^2\} \quad \text{(low frequency component)}$$

$$\Psi(\boldsymbol{\psi},\mathbf{c}) =\{\boldsymbol{\psi}_{2^j,l,\mathbf{k}}=2^{3j/4}\boldsymbol{\psi}(\mathbf{B}_l\mathbf{A}_{2^j}\mathbf{x}-\mathbf{M}_c\mathbf{k}),\ j>0, |l|\le\lceil 2^{j/2}\rceil, \mathbf{k}\in\mathbb{Z}^2\} \text{ (horizontal cone)}$$

$$\tilde{\Psi}(\tilde{\boldsymbol{\psi}},\mathbf{c}) =\{\tilde{\boldsymbol{\psi}}_{2^j,l,\mathbf{k}}=2^{3j/4}\tilde{\boldsymbol{\psi}}(\mathbf{B}_l^T\tilde{\mathbf{A}}_{2^j}\mathbf{x}-\tilde{\mathbf{M}}_c\mathbf{k}),\ j>0, |l|\le\lceil 2^{j/2}\rceil, \mathbf{k}\in\mathbb{Z}^2\} \text{ (vertical cone)}$$

$$\mathbf{M}_c=\begin{pmatrix} c_1 & 0\\ 0 & c_2\end{pmatrix}, \tilde{\mathbf{M}}_c=\begin{pmatrix} c_2 & 0\\ 0 & c_1\end{pmatrix}.$$

The cone-adapted shearlet system induces the tiling of the frequency domain that looks almost polar, as shown in Fig. 1.

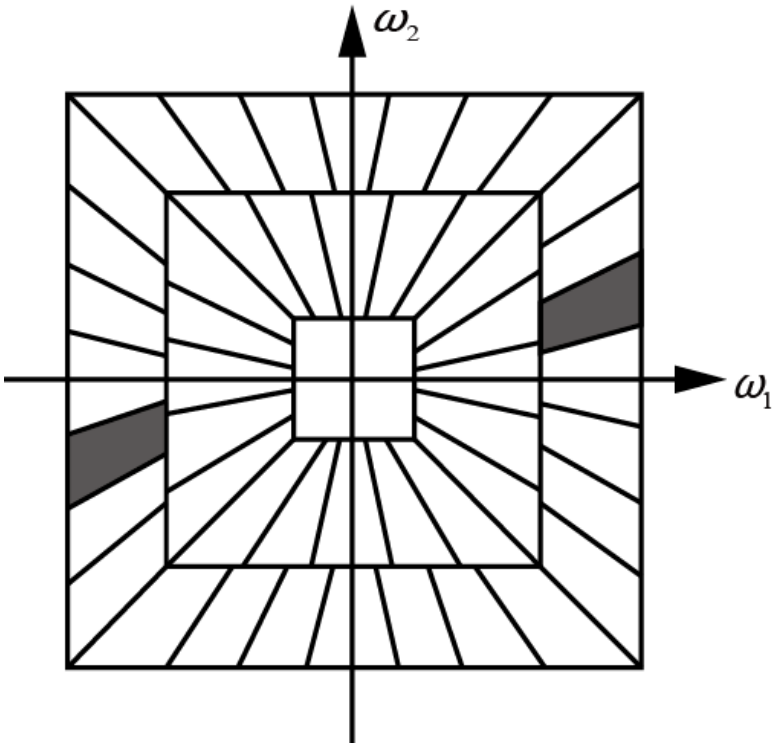

Fig. 1. Tiling of the frequency domain generated by the essential frequency support of a classical cone-adapted shearlet system. ω_1 and ω_2 are the frequency components of the horizontal and vertical direction, respectively.

Although the shearlet transform has many advantages such as sound theoretic basis and simple algorithm, it also has two less desirable aspects. First, the shearlet transform lacks shift invariance, which causes pseudo-Gibbs' artifacts during reconstructing images. In order to make the shearlet transform have the characteristics of shift invariance, Kutyniok and Labate (2007) proposed to replace the Laplace pyramid algorithm with the non-down-sampled one, but the redundancy of the non-down-sampled shearlet transform is greatly increased, which leads to large computation efforts. Second, the Laplace pyramid algorithm used in the shearlet

transform is a linear multi-scale decomposition method, and has a poorer ability to capture structural details. The non-linear multi-scale decomposition method can improve the ability to capture and preserve structural details.

Reisenhofer et al. (2016) modified the real shearlet transform and constructed the complex shearlets, which still yields local geometric information, but has certain desirable features that Fourier bases also have. In particular, the real parts of the generating functions are similar to be even-symmetric (like cosine) and the imaginary parts are odd-symmetric (like sine). In order to do this, the Hilbert transform is employed to construct the complex shearlet transform, which is shown as follows

$$S^{\mathrm{c}}(\boldsymbol{\varphi},\boldsymbol{\psi},\tilde{\boldsymbol{\psi}};\mathbf{c}) = \boldsymbol{\Phi}(\boldsymbol{\varphi},c_1) \cup \boldsymbol{\Psi}^{\mathrm{c}}(\boldsymbol{\psi},\mathbf{c}) \cup \tilde{\boldsymbol{\Psi}}^{\mathrm{c}}(\tilde{\boldsymbol{\psi}},\mathbf{c}) \quad , \tag{2}$$

where

$$\boldsymbol{\Phi}(\boldsymbol{\varphi},c_1)=\{\boldsymbol{\varphi}_m=\boldsymbol{\varphi}(\mathbf{x}-c_1\mathbf{k}),\mathbf{k}\in\mathbb{Z}^2\}$$

$$\boldsymbol{\Psi}^{\mathrm{c}}(\boldsymbol{\psi},\mathbf{c}) =\{\boldsymbol{\psi}^{\mathrm{c}}_{2^j,l.\mathbf{k}}=\boldsymbol{\psi}_{2^j,l.\mathbf{k}}+\mathrm{i}H_{\zeta_0}(\boldsymbol{\psi}_{2^j,l.\mathbf{k}})\}$$

$$\tilde{\boldsymbol{\Psi}}^{\mathrm{c}}(\tilde{\boldsymbol{\psi}},\mathbf{c}) =\{\tilde{\boldsymbol{\psi}}^{\mathrm{c}}_{2^j,l.\mathbf{k}}=\tilde{\boldsymbol{\psi}}_{2^j,l.\mathbf{k}}+iH_{\zeta_0}(\tilde{\boldsymbol{\psi}}_{2^j,l.\mathbf{k}})\} \quad ,$$

where $H_{\zeta_0}(\cdot)$ expresses the partial Hilbert transform, ζ_0 is $(1\ \ 0)^{\mathrm{T}}$ or $(0\ \ 1)^{\mathrm{T}}$.

Kutyniok et al. (2016) proposed a reliable digital implementation of the shearlet transform based on compactly supported frame. The sparse approximations provided by the algorithm yield the best results. Therefore, the complex shearlet transform can be implemented easily without increasing extra computation. The first row in Fig. 2(a) shows the frequency response of the conventional shearlet, the second row is the corresponding response of the complex shearlets. Fig. 2(b) shows the respective 2D shearlet filters corresponding to Fig. 2(a).

According to eq. (2), the discrete complex cone-adapted shearlet transform of the seismic data **u** can be expressed as

$$S^{\mathrm{c}}(\mathbf{u}) = (<\mathbf{u},\boldsymbol{\varphi}_m>,<\mathbf{u},\boldsymbol{\psi}^{\mathrm{c}}_{2^j,l.\mathbf{k}}>,<\mathbf{u},\tilde{\boldsymbol{\psi}}^{\mathrm{c}}_{2^j,l.\mathbf{k}}>) \quad . \tag{3}$$

There are several kinds of implementation methods for the shearlet transform, but most of those focus on the band-limited case. These approaches are based on the Parseval frame and suffer from the drawbacks such as high complexity, various artifacts and insufficient spatial localization. Kutyniok et al. (2016) developed a low complexity algorithm based on non-separable, compactly supported shearlet generators (Kutyniok et al., 2016). According to the construction of the complex shearlet transform discussed above, its implementation is very similar to the real shearlet transform, almost without increasing any computational effort (Reisenhofer et al., 2016).

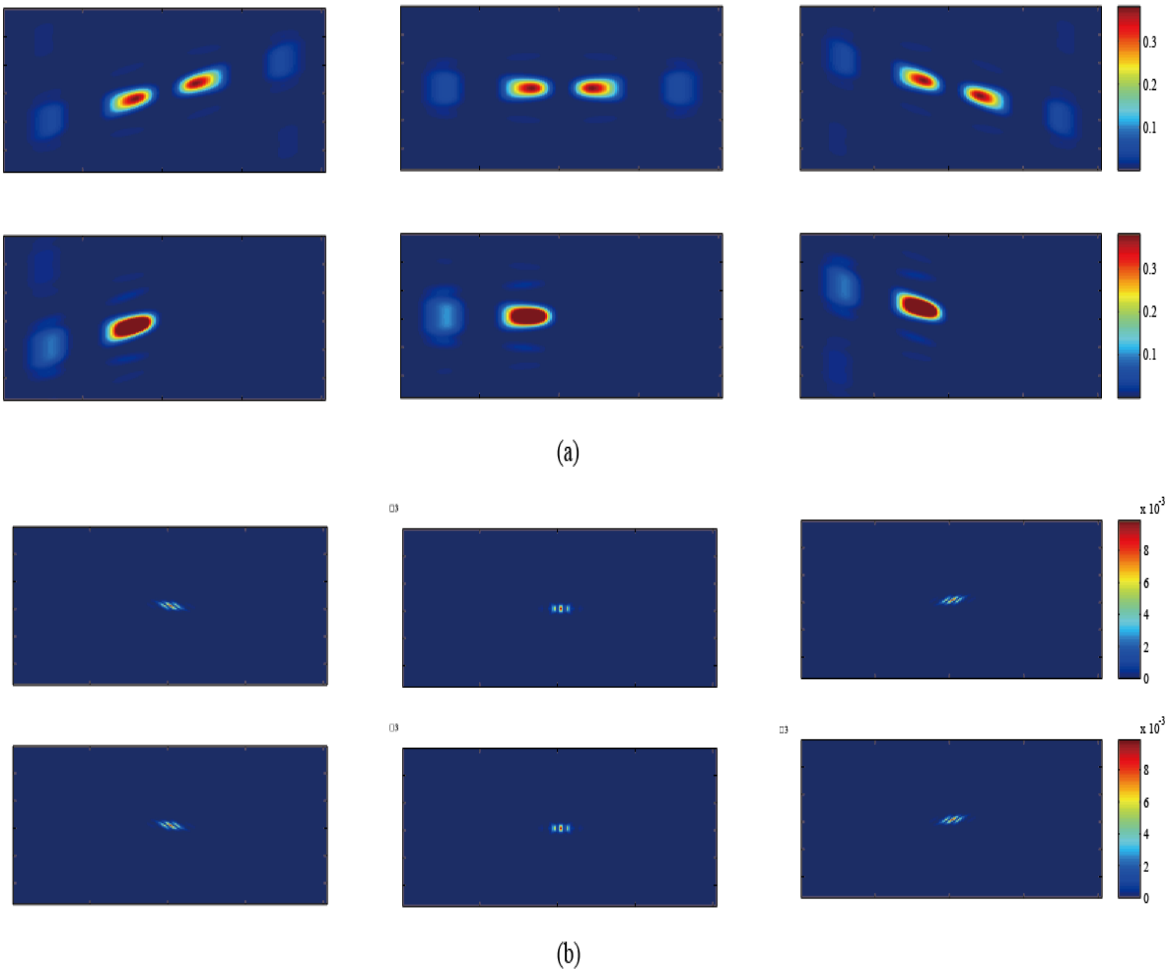

Fig. 2. (a) The shearlets in the wavenumber domain; (b) the shearlets in the spatial domain. In (a) and (b), the first row is corresponding to the real shearlets and the second row to the complex shearlets.

Block Coordinate Relaxation method

The regularly or irregularly sampled seismic data are usually expressed as

$$\mathbf{u}_s = \mathbf{M} \cdot \mathbf{u}_c , \tag{4}$$

where $\mathbf{u}_s$ is the observed data that contains the missing traces, $\mathbf{M}$ denotes the sampling matrix, $\mathbf{u}_c$ is the complete data. Based on the CS theory, the incomplete data $\mathbf{u}_s$ can be reconstructed through a sparse transform and a sparsity-promoting strategy. The complex shearlet transform is a multi-scale and multi-direction sparse transform, so that the incomplete seismic data $\mathbf{u}_s$ can be reconstructed by using the complex shearlet transform and a sparsity-promoting strategy. It is always ill-posed to solve eq. (4). Considering the sparsity of the seismic data $\mathbf{u}_c$ in the complex shearlet domain, the seismic data reconstruction is described as an optimization problem

$$\hat{\mathbf{x}} = \arg\min \|\mathbf{x}\|_p \quad s.t. \mathbf{M} \cdot S^{cT}(\hat{\mathbf{x}}) = \mathbf{u}_s \quad , \tag{5}$$

where $\mathbf{x}$ and $\hat{\mathbf{x}}$ represent the shearlet coefficient vector and its estimation respectively, p = 1 or 0 indicates L_1 or L_0 norm and S^{cT} denotes the inverse complex shearlet transform. Eq. (5) can be converted to a non–constrained optimization problem, and the objective function is defined as

$$J(\mathbf{x}) = \left\| \mathbf{u}_s - \mathbf{M} \cdot S^{cT}(\mathbf{x}) \right\|_2^2 + \lambda \cdot C(\mathbf{x}) \quad , \tag{6}$$

where λ is the regularization parameter, $C(\mathbf{x})$ indicates a sparsity constraint, such as the L_0 or L_1 norm constraint. The L_0 norm constraint is a NP (Non-deterministic Polynomial) problem, so the L_1 norm constraint is usually used to approximate the L_0 norm constraint. The L_1 regularization can lead to a parsimonious representation of signal $\mathbf{u}_s$ and can achieve super-resolution of the signal in time and frequency. Chen et al. (1996) built the concept of "Basis Pursuit" to solve the L_1 regularization and proposed the primal-dual log-barrier interior point (IP) algorithm by means of converting the primal problem into a quadratic programming problem. Bruce et al. (1998) proposed the BCR method to solve the basis pursuit based de-noising problem, which has the advantages of simplicity and rapid convergence speed compared to the IP algorithm. The method has been used widely in fitting log-linear models (Bishop et al., 1975), image reconstruction using regularized objective functions (Starck et al., 2005), Bayesian estimation of auto regressive models (Alliney and Ruzinsky, 1994).

The sparsity-promoting algorithm used in the paper is based on BCR, with some required changes due to adopting the complex shearlet transform and using the sampling matrix. The iteration formulation of the data reconstruction is expressed as follows:

$$\begin{aligned} &\mathbf{R} = \mathbf{M} \cdot (\mathbf{u}_s - \mathbf{u}_k) \\ &\mathbf{u}_{k+1} = \mathbf{u}_s + (\mathbf{I} - \mathbf{M}) \cdot S^{c\,T}(\boldsymbol{T}_{\tau_k}(S^{c}(\mathbf{u}_k + \mathbf{R}))) \end{aligned} \quad , \tag{7}$$

where $\mathbf{u}_k$ denotes the k-th iterative solution, S^c denotes the forward complex shearlet transform , $\boldsymbol{T}_{\tau_k}(\bullet)$ is the soft shrinkage function and is defined by

$$\boldsymbol{T}_{\tau_k}(x) = \frac{x}{|x|} \cdot (|x| - \tau_k)_+ , \tag{8}$$

where τ_k is a threshold. The algorithm is described as follows:

Algorithm 1 Seismic data reconstruction based on the complex shearlet transform using the BCR method

Input: the observed data $\mathbf{u}_s$, the measuring matrix $\mathbf{M}$, the number of iterations N, error *eps*.

Output: the reconstructed data $\tilde{\mathbf{u}}_c$.

1. Set up the complex shearlet transform parameters: scales, the level of shearing at each scale.
2. Initialization: compute the complex shearlet transform coefficients of $\mathbf{u}_s$ to select an initialized threshold τ_0; let $\mathbf{u}_0 = \mathbf{u}_s$.
3. For k =1 to N
4. Calculate the residual $\mathbf{R}_{k-1} = \mathbf{M} \cdot (\mathbf{u}_s - \mathbf{u}_{k-1})$.
5. Calculate the complex shearlet transform of $(\mathbf{u}_{k-1} + \mathbf{R}_{k-1}) : \mathbf{x}_{k-1} = S^C(\mathbf{u}_{k-1} + \mathbf{R}_{k-1})$.
6. Soft threshold the coefficient $\mathbf{x}_{k-1}$: $\tilde{x}_k = \boldsymbol{T}_{\tau_k}(\boldsymbol{x}_{k-1})$, $\boldsymbol{T}_{\tau_k}(\cdot)$ is the soft shrinkage function.
7. Apply the inverse complex shearlet transform to the thresholded coefficients to obtain the reconstructed data: $\mathbf{u}_k = S^{cT}(\tilde{\mathbf{x}}_k)$.
8. Reinsert the original traces $\mathbf{u}_s$ to the reconstructed traces: $\mathbf{u}_k = \mathbf{u}_s + (\mathbf{I} - \mathbf{M}) \cdot \mathbf{u}_k$.
9. $\tau_k = f(\tau_{k-1})$, $f(\cdot)$ is the linear or exponential threshold function.
10. If $k \le N$ or the reconstructed error > *eps*
11. then go to step 3
12. Else
13. Output the reconstructed data: $\tilde{\mathbf{u}}_c = \mathbf{u}_k$.
14. End
15. Return

In the above algorithm, if $C(\mathbf{x})$ in eq. (6) is the L_1 sparsity constraint, the soft threshold is used. However, replacing the soft threshold by a hard one towards the end of the iterative process may have better results because the L_1 norm constraint is only a good approximation for the desired L_0 one.

NUMERIC EXAMPLES

First, synthetic seismic data sets are selected to prove the validity of the proposed method. Second, numerical examples using real seismic data further demonstrate the performance in a realistic setting. In order to evaluate the reconstructed performance, the SNR, which indicates the error between the reconstructed data and the original data, is defined. The recovered SNR is expressed as

$$SNR = 10\log_{10}\left(\frac{\left\|\mathbf{u}_{\text{orig}}\right\|_2}{\left\|\mathbf{u}_{\text{orig}} - \mathbf{u}_{\text{rect}}\right\|_2}\right)^2 \quad , \tag{9}$$

where $\mathbf{u}_{\text{orig}}$ denotes the complete seismic data and $\mathbf{u}_{\text{rect}}$ is the reconstructed data.

SYNTHETIC DATA

Fig. 3a is a synthetic seismic shot, which is generated with a finite-difference code for a subsurface velocity model with 2D inhomogeneities. The number of traces is 256, and the interval between traces is 15 m, the temporal sampling is 4 ms. The data sets with 50% and 70% traces missing, based on a jittered sampling, are shown as Figs. 3b–c. Figs. 3d-f show the *f-k* spectrum corresponding to (a)-(c), respectively.

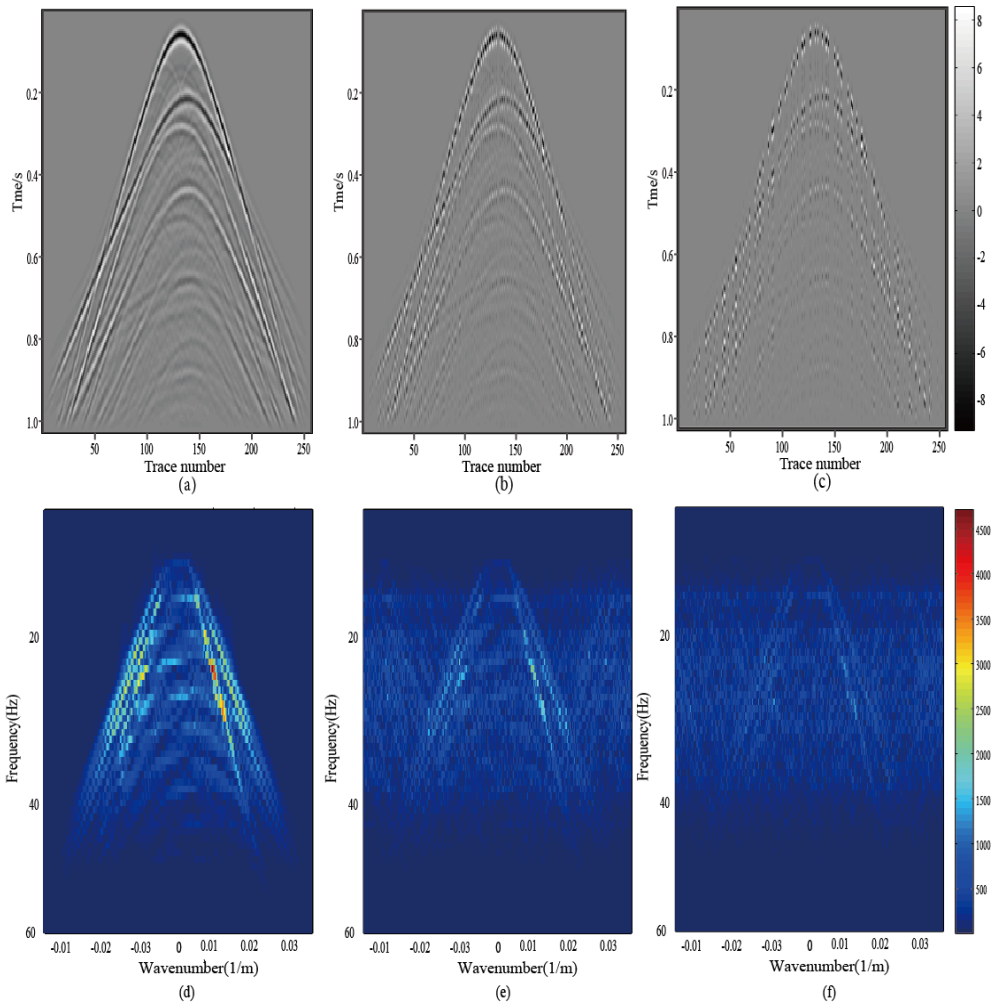

Fig. 3. The complete data and irregularly sampled seismic data. (a) The complete data; (b) the irregular data with 50% traces missing; (c) the irregular data with 70% traces missing. (d)-(f) are the *f-k* spectrum corresponding to (a)-(c).

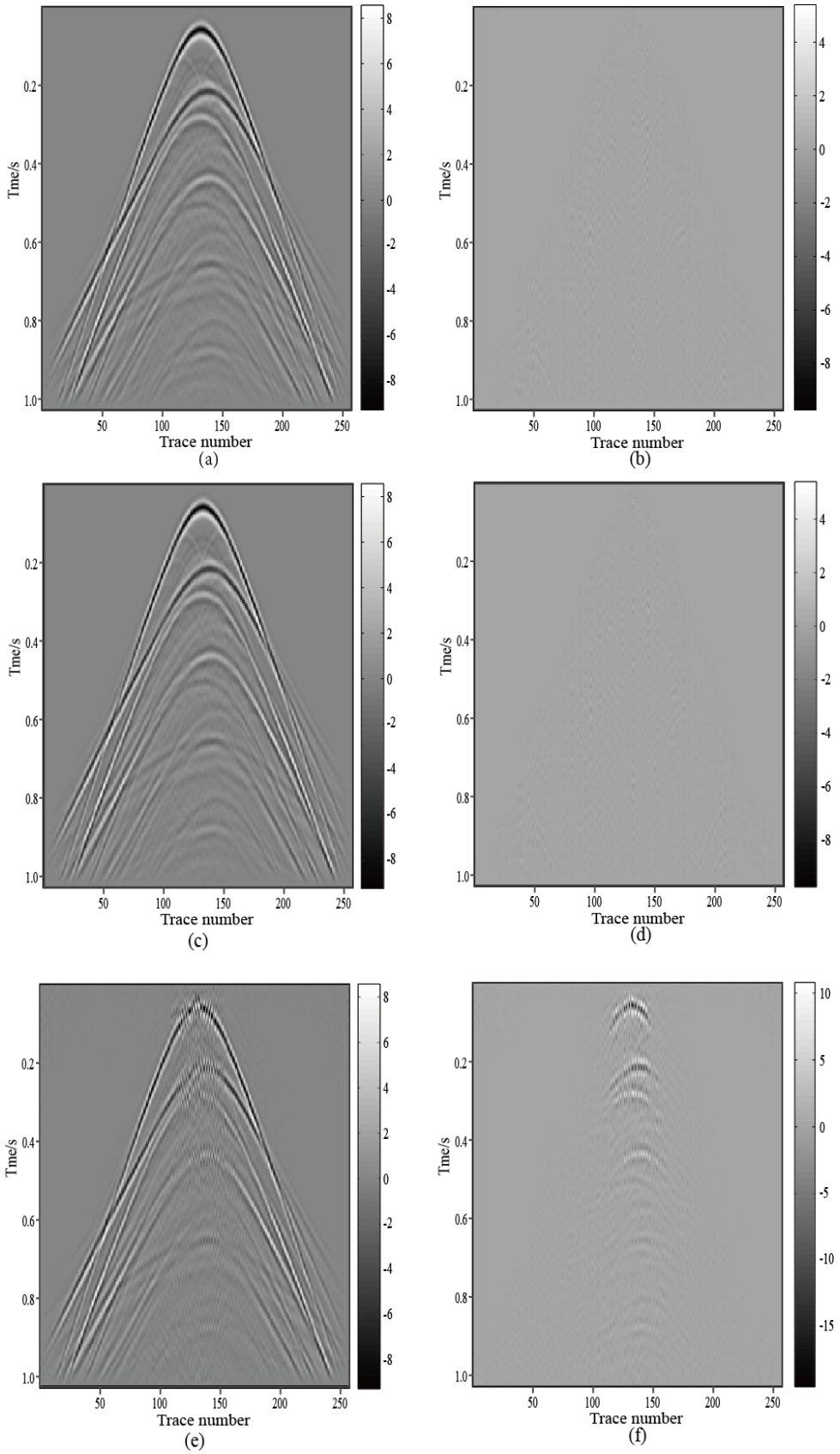

Fig. 4. The reconstructed data (left column) and the corresponding residuals (right column) when 50% traces are missing (see Fig. 3b). The first row is for the complex shearlet-based method, the second row is for the real shearlet-based method and the third row is for the curvelet-based method.

Figs. 4 and 6 demonstrate the reconstruction results and residuals based on the complex shearlet and the real shearlet transform for every choice of missing traces, while the reconstruction results and residuals based on the curvelet transform are also shown. As expected, it shows that when the number of missing traces increases, the residual increases. It can be seen that the reconstructed data using the complex shearlet–based method agree better with the complete data shown in Fig. 3a than that using the real shearlet-based and curvelet-based method.

Figs. 5 and 7 show the corresponding *f-k* spectrum of the reconstructed data sets. The aliases are suppressed effectively for the three transforms, but the shearlet-based methods are obviously superior to the curvelet-based. For the case of 50% missing traces (Fig. 5), the *f-k* spectra of the reconstructed data using the real and complex shearlet transform are almost same, and so are the reconstructed data sets shown in Fig. 4.

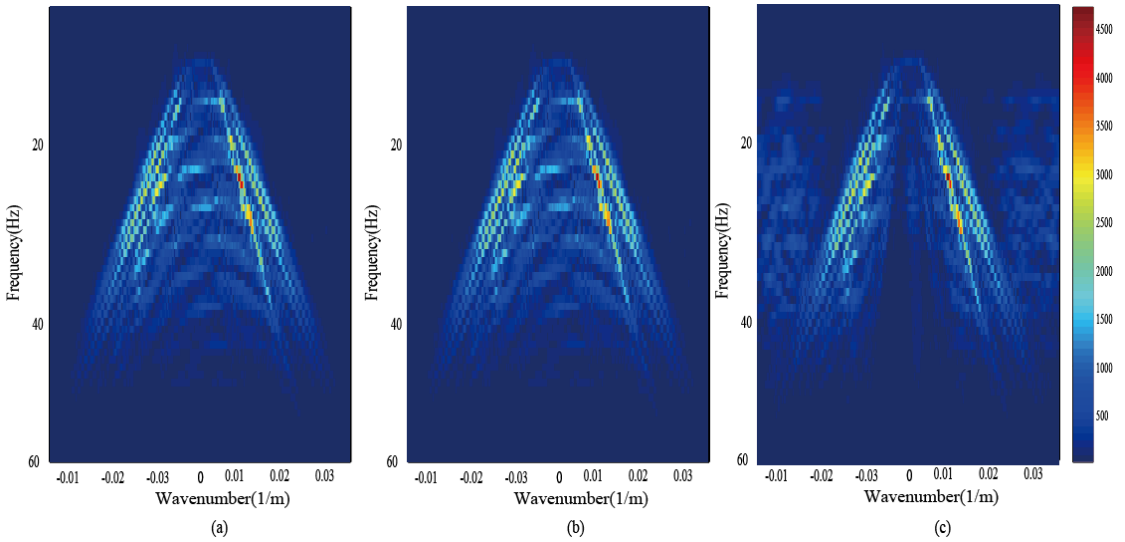

Fig. 5. The *f-k* spectrum of the reconstructed data corresponding to Fig. 4 (a), (c) and (e).

As shown in Fig. 7, when the amount of traces missing is 70%, the *f-k* spectrum corresponding to the complex shearlet transform is somewhat stronger than that corresponding to the real shearlet transform, especially for the areas in the red circles. This indicates a better reconstruction results, as can be verified in Fig. 6. It also can be seen from Figs. 6 and 7 that the curvelet-based method can not reconstruct data effectively with such large number of missing traces. In order to further compare the reconstruction performance, the SNR curves as a funcation of the iterations are plotted in Fig. 8.

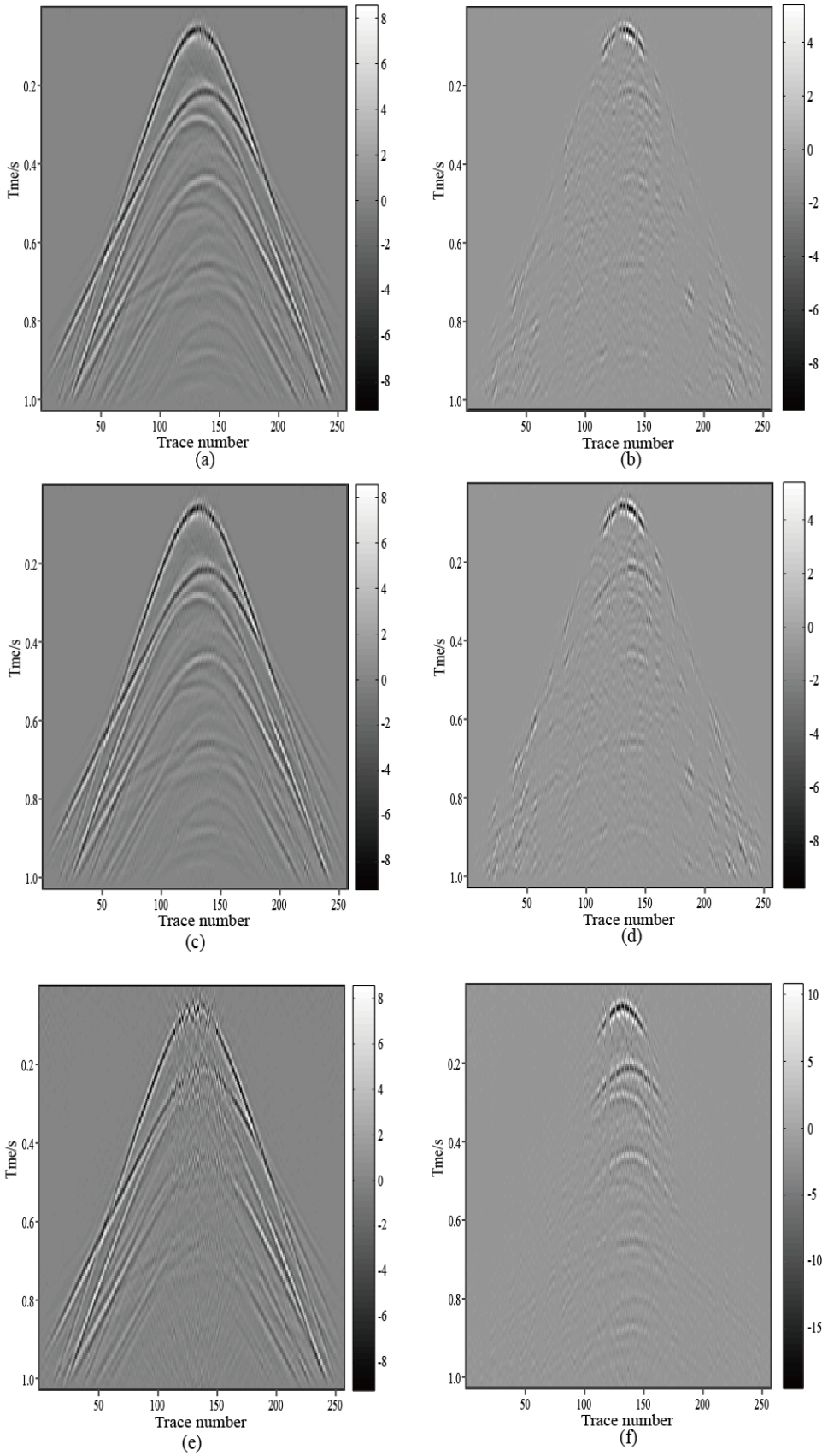

Fig. 6 The reconstructed data (left column) and the corresponding residuals (right column) when 70% traces are missing (see Fig. 3c). The first row is for the complex shearlet-based method, the second row is for the real shearlet-based method and the third row is for the curvelet-based method.

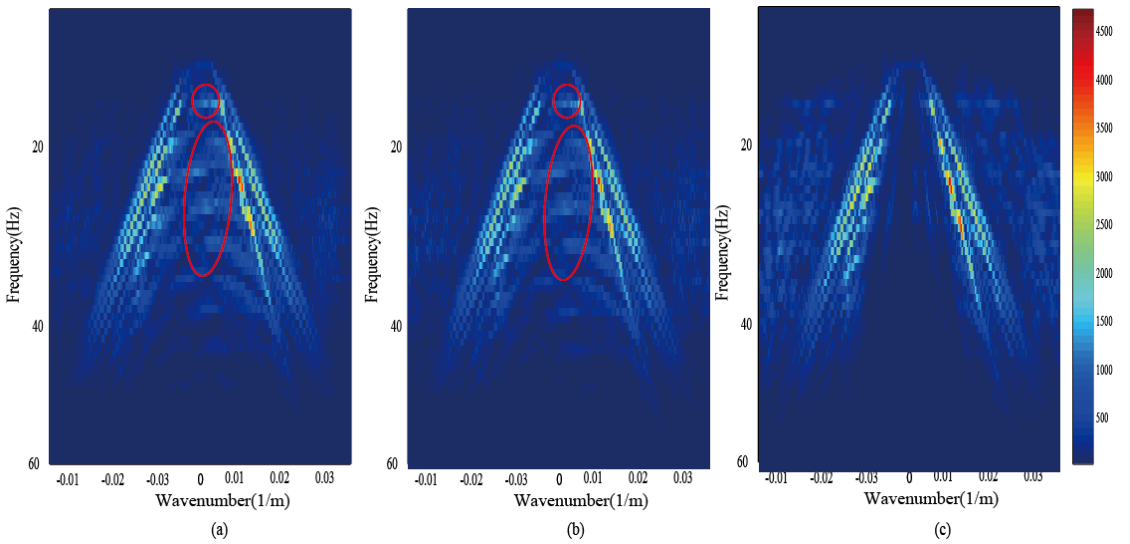

Fig. 7. The *f-k* spectrum of the reconstructed data corresponding to Fig. 6 (a), (c) and (e).

Fig. 8 indicates the complex shearlet based method is superior to the real shearlet-based and the curvelet-based method and the recovered SNR is lower as the missing traces increase. The final SNRs are 25.92 dB and 12.39 dB using the complex shearlet transform with 50% and 70% traces missing, respectively. The SNRs corresponding to the real shearlet are 25.25 dB and 10.52 dB and the SNRs corresponding to the curvelet transform are 23.23 dB and 4.76 dB. Performance for the synthetic seismic data prove that the complex shearlet based method has a better reconstruction ability compared to the other methods when the number of missing traces is growing.

Real data application

The real post–stack seismic data from an oilfield is utilized to further confirm the validity of the proposed method. Fig. 9a shows the complete data with 201 traces and the 1501 samples in each trace, in which the temporal sampling interval is 2 ms. The incomplete data sets with 50% and 70% traces missing using a jittered under–sampling approach are shown in Figs. 9b-c. For convenience of comparison, we test each method with the same parameters of the BCR algorithm. The reconstructed results and residuals are shown in Figs. 10-11.

When the amount of traces missing is 50%, the reconstructed results using the complex shearlet and the real shearlet transform have almost the same performance and agree well with the complete data shown in Fig. 9a, and both methods are superior to the curvelet-based method, although the complex shearlet-based method is slightly better than the real shearlet-based method. But when the number of traces missing is 70%, the complex shearlet-based method clearly outperforms both the real shearlet-based and curvelet-based method, especially for the time interval of 0.8-2.0 s. To further compare the performances, the SNR curves with iterations for the data sets are shown in Fig. 12.

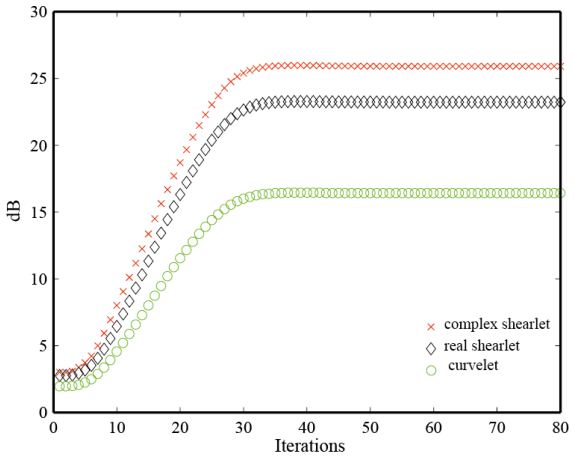

(a)

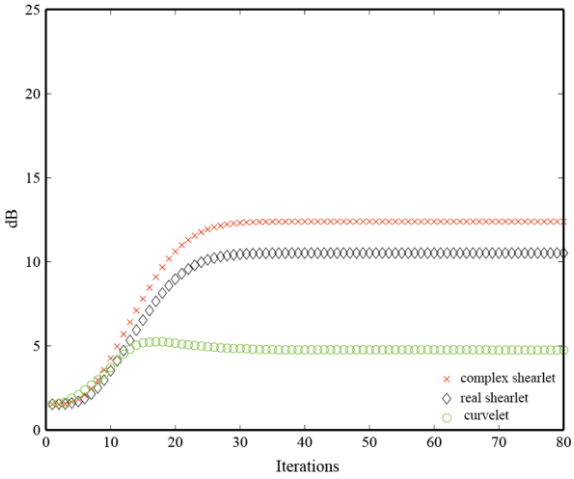

(b)

Fig. 8. SNRs with iterations. (a)-(b) is corresponding to the case of 50% and 70% traces missing, respectively.

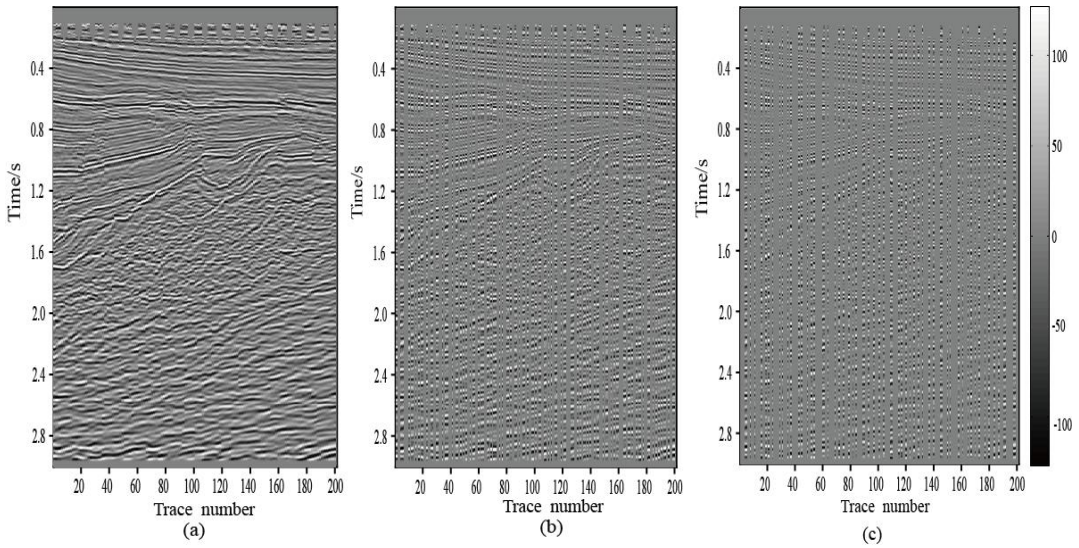

Fig. 9. (a) The complete field data and irregularly sub-sampled seismic data. (b) The complete data; the irregular data with 50% traces missing; (c) the irregular data with 70% traces missing.

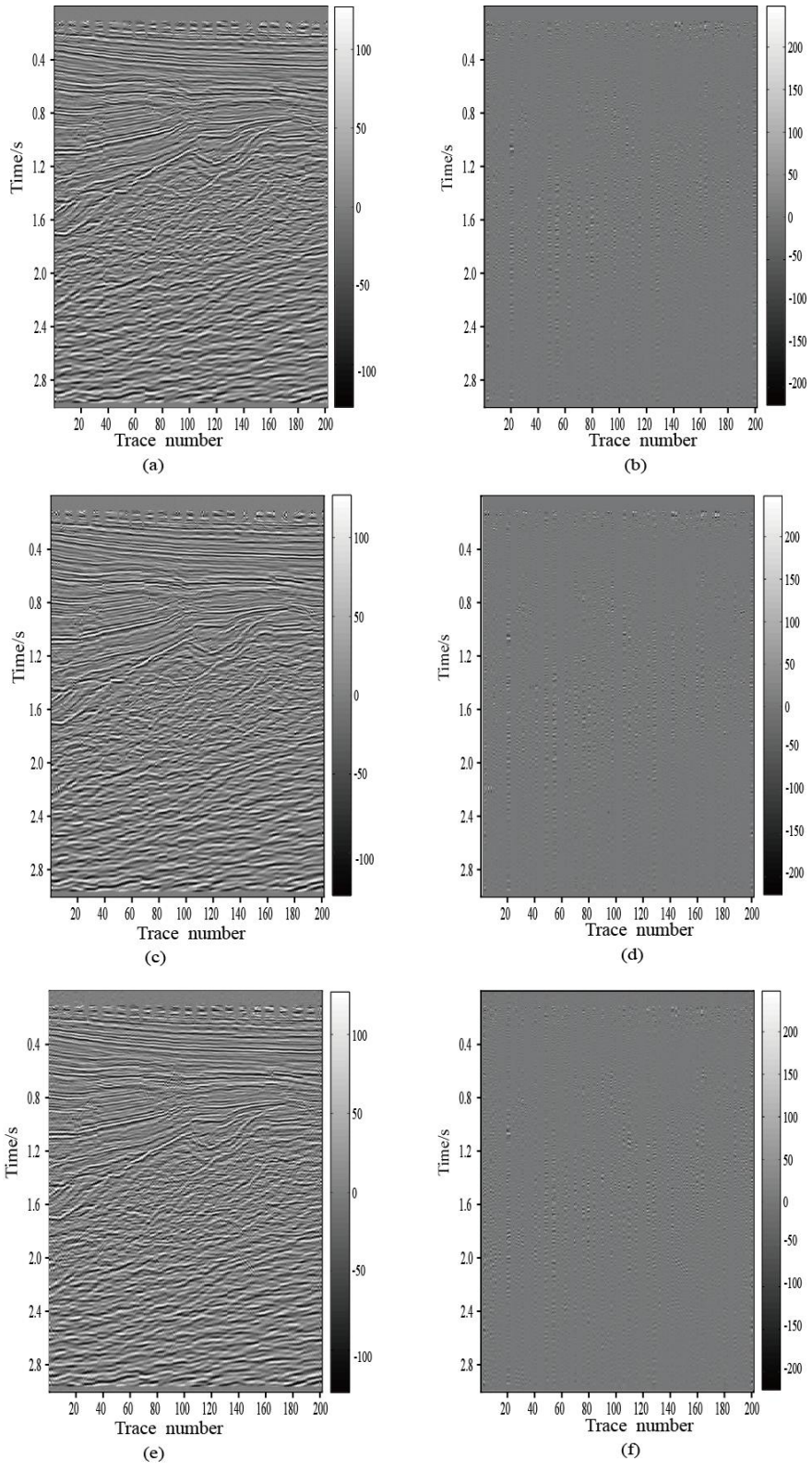

Fig. 10. The reconstructed data (left column) and the corresponding residuals (right column) when 50% traces are missing. The first row is for the complex shearlet-based method, the second row is for the real shearlet-based method and the third row is for the curvelet-based method.

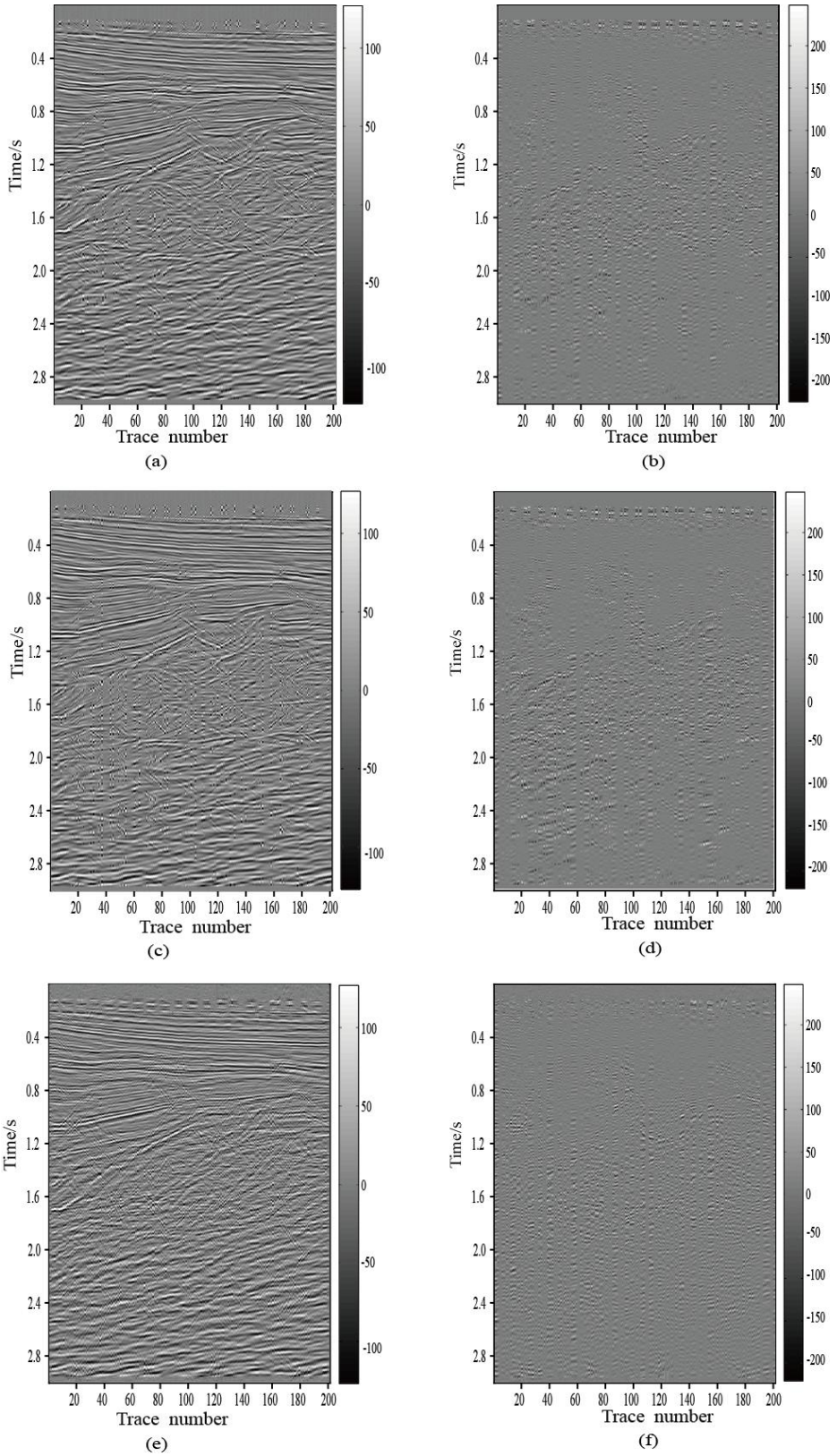

Fig. 11. The reconstructed data (left column) and the corresponding residuals (right column) when 70% traces are missing. The first row is for the complex shearlet-based method, the second row is for the real shearlet-based method and the third row is for the curvelet-based method.

Fig. 12 indicates that results based on the complex shearlet transform are again superior to the other two methods. From the SNR curves shown in Fig. 12, we can conclude that the complex shearlet transform is sparser and the performance is better compared to the real shearlet and the curvelet transform for the real seismic data example.

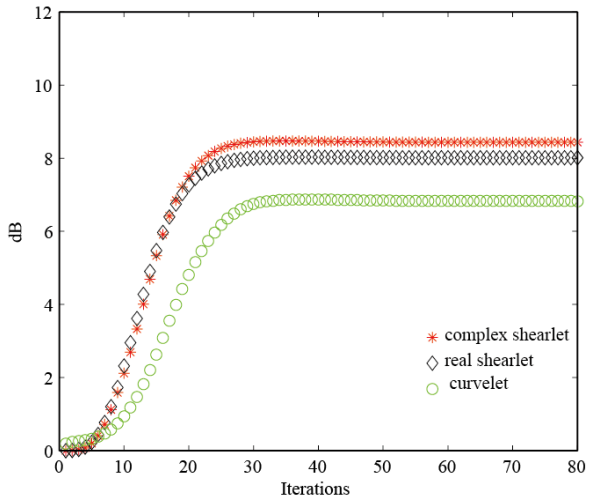

(a)

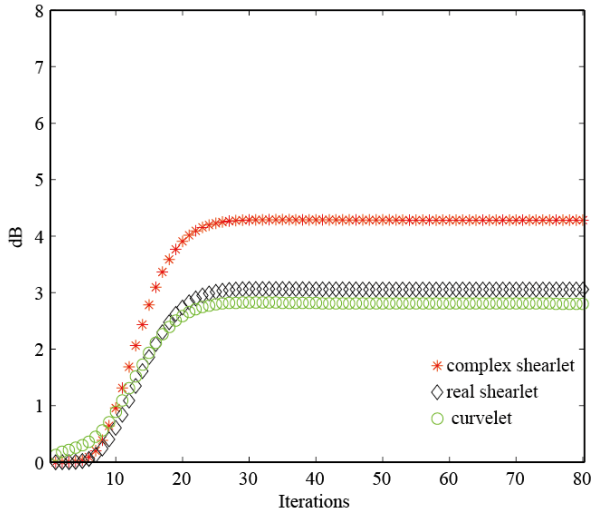

(b)

Fig. 12. SNRs with iterations for the field data. (a)-(b) is corresponding to the case of 50% and 70% traces missing,

From the reconstructed results of the synthetic and the real data sets, we can draw a rough conclusion that the method based on the complex shearlet transform using BCR is efficient. It also can be seen from Figs. 8 and 12 that when the maximum iteration number is 80, the recovered SNRs are stable and the curves become almost horizontal after nearly 20-30 iterations for the synthetic data, which means that the quality of the reconstructed seismic data improves very little after 20-30 iterations, while for the real data, the number of required iterations is about 30-40.

DISCUSSION

The advantage of the complex shearlet transform compared to the real shearlet transform

The complex shearlet transform is based on the complex-valued functions shown as

$$\psi^{c} = \psi^{even} + i\psi^{odd} \quad , \tag{10}$$

where ψ^{even} is an even-symmetric real-valued shearlet which has the possibly anisotropic support constructed by applying shearing, scaling and translation operators to a wavelet-like generating function, and ψ^{odd} is the Hilbert transform of ψ^{even}. Such construction makes the shearlet-based multi-scale representation systems conceptually closer towards the classical Fourier basis. So the complex shearlet transform not only has the multi-resolution, multi-direction, anisotropic and favorable spatial and frequency localization, but also has the shift invariance to the magnitude response. Therefore, the complex shearlet transform can capture the geometric characteristic more effectively compared to the real shearlet transform, the wavelet transform and the curvelet transform.

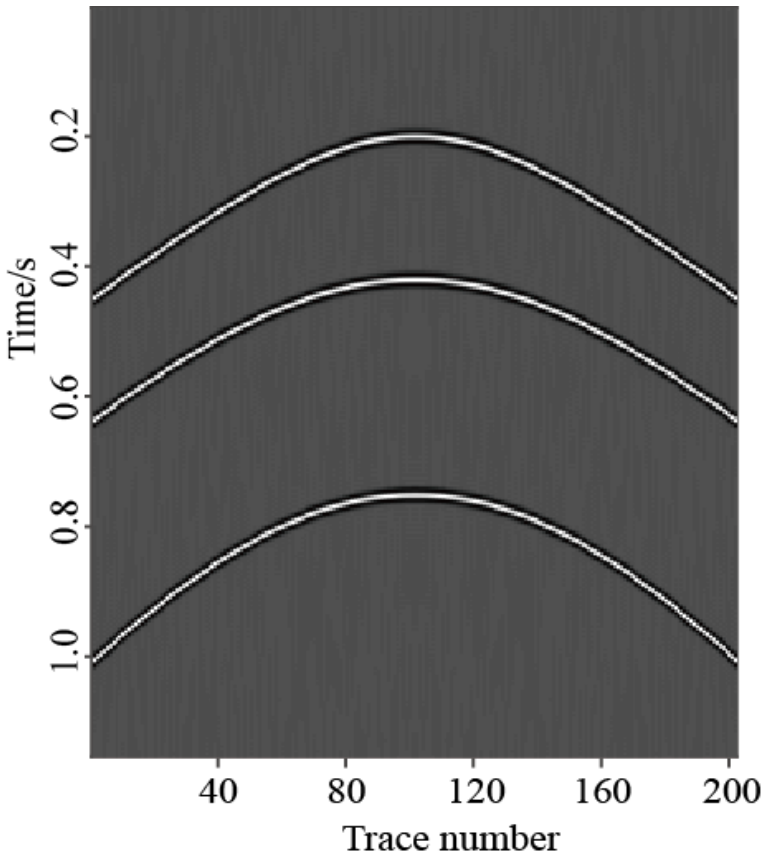

Fig.13. The synthetic data of a three-layer model.

To illustrate this, Fig. 13 shows the synthetic seismic data of a simple three-layer model. Fig. 14 demonstrates the real shearlet and the complex shearlet coefficients of the synthetic seismic data. It can be seen from Fig. 14 that the coefficients amplitude of the complex shearlet transform is greater than that of the real shearlet transform. Analysis reveals that the coefficients of the real shearlet transform are still real-valued and may produce certain shift variance. So, a smaller shift of the location of the reflected wave will result in a bigger variation of the coefficients of the real shearlet transform, which damages the information of the signal and leads to worse reconstruction results. The coefficients of the complex shearlet transform are complex-valued and the amplitudes do not vary with shifting, so the principle character of a signal can be preserved and the reconstructed results have higher signal to noise ratio.

Performance comparison of POCS and BCR methods

Among the sparsity-promoting strategies for reconstructing irregularly sampled seismic data, the POCS method has been applied widely because it is easy to be implemented and generally performs well. The BCR algorithm, which is first proposed for solving the Basis Pursuit de-noising problem, is broadly applicable and conceptually simple. We compare the performance of the BCR and POCS algorithms using the complex shearlet transform to reconstruct the seismic data. The synthetic data from Fig. 3b is selected with the 50% traces missing. The parameters of the two algorithms such as iterations, threshold condition and convergence errors are configured to be the same. Fig. 15 shows the SNR curves of the two algorithms. At the initial iterations, the performance of the BCR is superior to that of POCS. The SNR of BCR is stable at about 30 iterations, while the POCS is stable after about 40 iterations. So we can see that the BCR algorithm has a faster convergence than POCS.

Although the complex shearlet transform has better performance compared to other transforms, there are still some problems that need to be considered further, such as the noisy or anti-aliasing seismic data reconstruction using the complex shearlet transform, 3D data cube reconstruction by developing a 3D complex shearlet transform, and using a more efficient optimization algorithm.

CONCLUSION

In this paper, the irregularly sampled seismic data is reconstructed via the complex shearlet transform and the BCR algorithm. Using the Hilbert transform, we construct the complex shearlets, which have shift invariance features and are better suited for handling geometric structures in multi-dimensional data than using real shearlets. We utilize the BCR algorithm that has a global and fast convergence characteristic as a sparsity-promoting strategy. We also analyze the advantage of the complex shearlet transform compared to the real shearlet and the curvelet transform

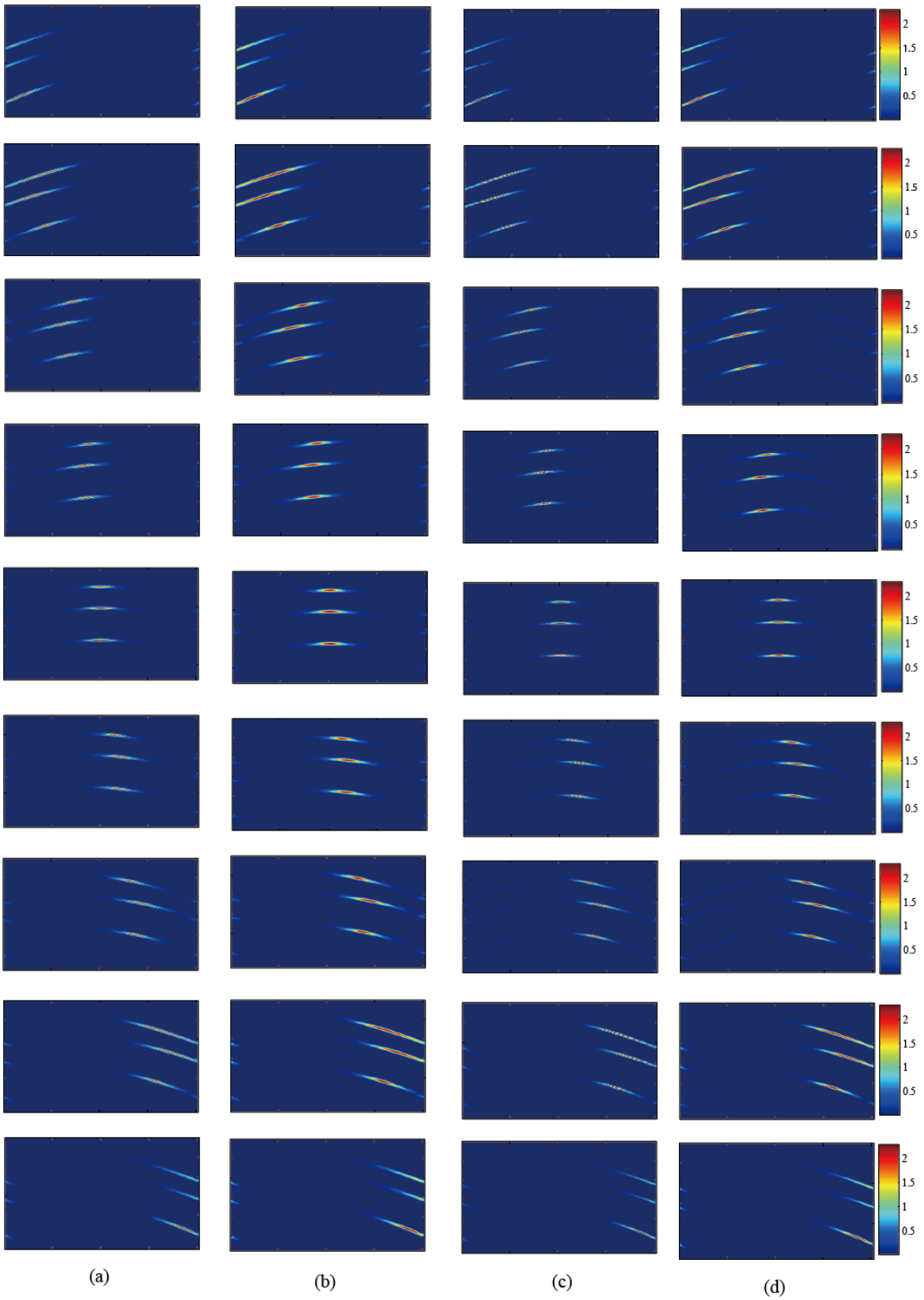

Fig. 14. The real shearlet and complex shearlet coefficients of the synthetic seismic data shown in Fig. 13. (a) and (c) are the coefficients of the real shearlet on the third and fourth scale, respectively. (b) and (d) are the corresponding complex shearlet. Nine shearing directions are selected from each scale. The parameters of the shearlet system are: the number of scales is 4, the level of shearing occuring on each scale is [1 1 2 2].

and compare the performance of the BCR and POCS algorithms. The numerical experiments on synthetic and real data with different under-sampling rates demonstrate the validity of the proposed method, which has more superiority than the other methods, especially when the amount of traces missing is increasing.

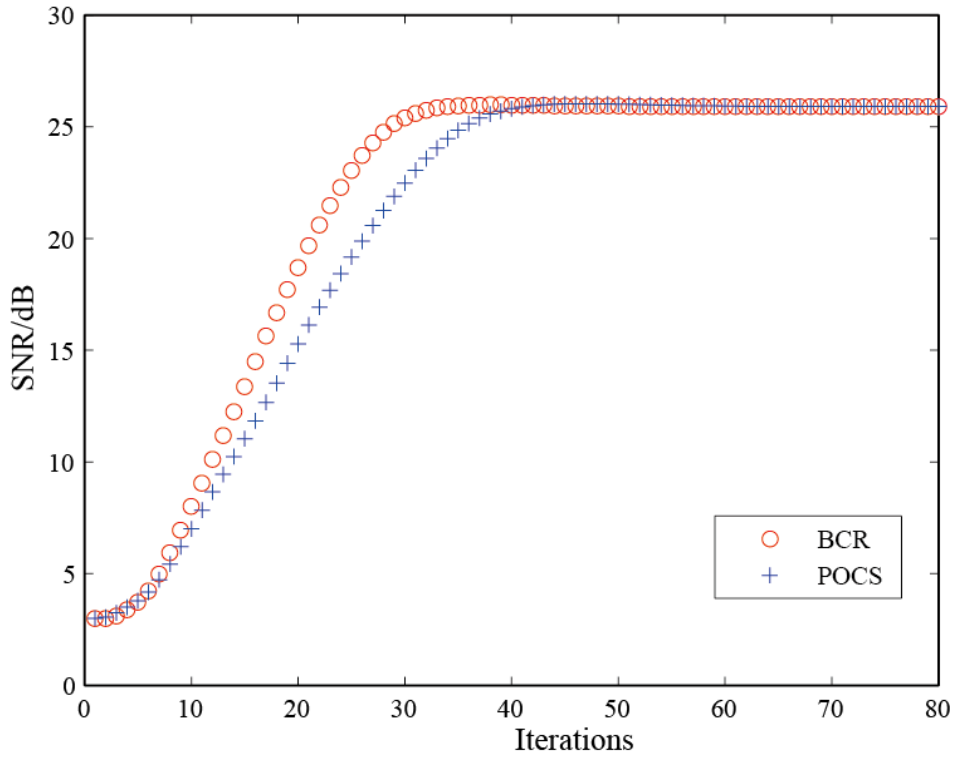

Fig. 15. Performance comparison of BCR and POCS.

ACKNOWLEDGMENTS

The authors would like to thank the editor and the comments made by the reviewer helped us to improve our paper. We also acknowledge the financial support of the Natural Science Foundation of the Jiangsu Higher Education Institutions of China (Grant No. 16KJB310001) and the Natural Science Foundation of Jiangsu Province of China (BK20170436).

REFERENCES

Abma, R. and Kabir, N., 2006. 3D interpolation of irregular data with a POCS algorithm. Geophysics, 71(6): E91-E97.

Alliney, S. and Ruzinsky, S.A., 1994. An algorithm for the minimization of mixed l_1 and l_2 norm with application to Bayesian estimation. IEEE Transact. Signal Process., 42: 618-627

Bishop, Y.M.M., Fienberg, S.E. and Holland, P.W., 1975. Discrete Multivariate Analysis: Theory and Practice. MIT Press, Cambridge, MA.

Bruce, A., Sardy, S. and Tseng P., 1998. Block coordinate relaxation methods for nonparametric signal de-noising. Proc. SPIE - The International Society for Optical Engineering, 3391: 75-86.

Cao, J., Wang, Y., Yang, C. and Zhao, J., 2011. A review on restoration of seismic wavefields based on regularization and compressive sensing. Inverse Probl. Sci. Engineer., 19: 679-704.

Cao, J., Wang, Y. and Yang, C., 2012. Seismic data restoration based on compressive sensing using the regularization and zero-norm sparse optimization. Chin. J. Geophys., 55: 596-607.

Cao, J. and Wang, Y., 2014. Seismic data restoration with a fast L_1 norm trust region method. J. Geophys. Engineer., 11: 045010.

Cao, J., Wang, Y. and Wang, B., 2015a. Accelerating seismic interpolation with a gradient projection method based on tight frame property of curvelet. Explor. Geophys., 43: 253-260.

Cao, J. and Zhao, J., 2015b. 3D seismic interpolation with a low redundancy, fast curvelet transform. J. Seismic Explor., 24: 121-134.

Cao, J. and Wang, B., 2015c. An improved projection onto convex sets methods for simultaneous interpolation and denoising. Chin. J. Geophys. (in Chinese), 58: 2935-2947.

Candès, E. and Donoho, D.L., 2004. New tight frames of curvelets and optimal representation of objects with C_2 singularities. Comm. Pure Appl. Math., 57: 219-266.

Chemingui, N. and Biondi, B., 2002. Seismic data reconstruction by inversion to common offset. Geophysics, 67: 1575-1585.

Chen, S., Donoho, D.L. and Saunders, M., 1996. Atomic decomposition by basis pursuit Tech. Report, Stanford University.

Easley, G., Labate, D. and Lim, W.Q., 2008. Sparse directional image representations using the discrete shearlet transform. Appl. Computat. Harmon. Analys., 25: 25-46.

Feng, F., Wang, Z., Liu, C. and Wang, D., 2016. Seismic data reconstruction based on sparse constraint in the shearlet domain. Geophys. Prosp. Petrol., 55: 682-691.

Fomel, S., 2003. Seismic reflection data interpolation with differential offset and shot continuation. Geophysics, 68: 733-744.

Gao, J., Chen, X., Li, J., Liu, G.C. and Ma, J., 2010. Irregular seismic data reconstruction based on exponential threshold model of POCS method. Appl. Geophys. 72: 229-238.

Gao, J., Sacchi, M. and Chen, X., 2013. A fast reduced-rank interpolation method for prestack seismic volumes that depend on four spatial dimensions. Geophysics, 78(1): V21-V30.

Genzel, M. and Kutyniok, G., 2014. Asymptotic analysis of inpainting via universal shearlet systems. SIAM J. Imag. Sci., 7: 2301-2339.

Glenn, R.E., Demetrio, L. and Flavia, C., 2009. Shearlet-based total variation diffusion for denoising. IEEE Transact. Image Process., 18: 260-268.

Guo, J.Y., Zhou, X.Y. and Yu, S.P., 1996. Iso-interval trace interpolation in F-X domain. OGP, 31: 28-34.

Guo, K., Kutyniok, G. and Labate, D., 2006. Sparse multidimensional representations using anisotropic dilation und shear operators. Wavelets and Splines, Athens, GA. TN: 189-201.

Hennenfent, G. and Herrmann, F.J., 2008. Simply denoise: wavefield reconstruction via jittered under-sampling. Geophysics, 73(3): V19-V28.

Herrmann, F.J. and Hennenfent, G., 2008. Non-parametric seismic data recovery with curvelet frames. Geophys. J. Internat., 173: 233-248.

Kong, D. and Peng, Z., 2015. Seismic random noise attenuation using shearlet and total generalized variation. J. Geophys. Engineer., 12: 1024-1035.

Kutyniok, G. and Labate, D., 2007. Optimally sparse multidimensional representation using shearlets. SIAM J. Mathemat. Analys., 39: 298-318.

Kutyniok, G. and Labate, D., 2009. Resolution of the wavefront set using continuous shearlets. Transact. Am. Mathemat. Soc., 361: 2719-2754.

Kutyniok, G. and Labate, D., 2012. Introduction to Shearlets: Multiscale Analysis for Multivariate Data. Springer Verlag, New York.

Kutyniok, G., Shahram, M. and Zhuang, X.S., 2012. ShearLab: A rational design of a digital parabolic scaling algorithm. SIAM J. Imag. Sci., 5: 1291-1332.

Kutyniok, G. and Petersen, P., 2015. Classification of edges using compactly supported shearlets. Appl. Comput. Harmon. Anal., 42: 245-293.

Kutyniok, G., Lim, W.Q. and Reisenhofer, R., 2016. Shearlab 3D: faithful digital shearlet transforms based on compactly supported shearlets. ACM Transact. Mathemat. Softw., 42(5): 1-42.

Lim, W.Q., 2010. The discrete shearlets transform: a new directional transform and compactly supported shearlets transform. IEEE Transact. Image Process., 19: 1166-1180.

Liu, J.C., Chou, Y.X. and Zhu, J.J., 2018. Interpolating seismic data via the POCS method based on shearlet transform. J. Geophys. Engineer., 15: 852-876.

Liu, Y., Zhang, P. and Liu, C., 2017**.** Seismic data interpolation using generalised velocity-dependent seislet transform. Geophys. Prosp. 65(S1): 82-93.

Ma, J.W., 2013. Three-dimensional irregular seismic data reconstruction via low-rank matrix completion. Geophysics, 78(5): V181-V192.

Minh, N.D. and Vetterli, M., 2005. The contourlet transform: An efficient directional multiresolution image representation. IEEE Transact. Image Proc., 14: 2091-2106.

Naghizadeh, M. and Sacchi, M. D. 2007 Multistep autogressive reconstruction of seismic records Geophysics 72(6) V111-V118.

Naghizadeh, M. and Sacchi, M.D., 2009. F-x adaptive seismic-trace interpolation. Geophysics, 74(1): V9-V16.

Naghizadeh, M. and Innanen, K.A., 2011. Seismic data interpolation using a fast generalized Fourier transform Geophysics 76(1) V1-V10.

Nurul Kabir, M.M. and ,Verschuur, D.J., 1995. Restoration of missing offsets by parabolic Radon transform. Geophys. Prosp., 43: 347-368.

Ozkan, M., Tekalp, M. and Sezan, M., 1994. POCS-based restoration of space-varying blurred images. IEEE Transact. Image Process., 3: 450-454.

Patti, A., Sezan, M. and Tekalp, A., 1997. Superresolution video reconstruction with arbitrary sampling lattices and nonzereo aperture time. IEEE Transact. Image Process., 6: 1064-1076.

Pein, A., Loock, S., Plonka, G. and Salditt, T., 2016. Using sparsity information for iterative phase retrieval in x-ray propagation imaging. Opt. Express, 24: 8332-8343.

Pejoski, S., Kafedziski, V. and Gleich, D., 2015. Compressed sensing MRI using discrete nonseperable shearlet transform and FISTA. IEEE Sign. Process. Lett., 22: 1566-1570.

Porsani, M., 1999. Seismic trace interpolation using half-step prediction filters. Geophysics, 64: 1461-1467.

Reisenhofer, R., Kiefer, J. and King, E.J., 2016. Shearlet-based detection of flame fronts. Experim. Fluids, 57: 41.

Ronen, J., 1987. Wave equation trace interpolation. Geophysics, 52: 973-984.

Sheng, Y., Demetrio, L., Glenn, R.E. and Hamid, K., 2009. A shearlet approach to edge analysis and detection. IEEE Transact. Image Process., 18: 929-941.

Spitz, S., 1991. Seismic trace interpolation in the F-X domain. Geophysics, 56: 785-794.

Starck, J.L., Elad, M. and Donoho, D.L., 2005. Image decomposition via the combination of sparse representation and a variational approach. IEEE Transact. Image Process., 14: 1570-1582.

Wang, B., Wu, R., Geng, Y. and Chen, X., 2014. Dreamlet-based interpolation using POCS method. J. Appl. Geophys., 109: 256-265.

Wang, B., Wu, R., Chen, X. and Li, J., 2015. Simultaneous seismic data interpolation and denoising with a new adaptive method based on dreamlet transform. Geophys. J. Internat., 201: 1180-1192.

Wang, B., 2016. An Efficient POCS Interpolation method in the frequency-space domain. IEEE Geosci. Remote Sens. Lett., 13: 1384-1387.

Wang, B., Chen, X., Li, J. and Cao, J., 2016. An improved weighted Projection Onto Convex Sets method for seismic data interpolation and denoising. IEEE J. Select. Topics Appl. Earth Observat. Remote Sens., 9: 228-235.

Wang, Q., 2010. The discrete shearlet transform: a new directional transform and compactly supported shearlet frames. IEEE Transact., 19: 1166-1180.

Yang, P., Gao, J. and Chen, W., 2012. Curvelet-based POCS interpolation of nonuniformly sampled seismic records. J. Appl. Geophys., 79: 90-99.

Zhou, X., 1997. Seismic trace interpolation in F-X domain. Oil Geophys. Prosp., 32: 154-162.

Zhang, L., Han, L.G., Xu, D.X., Li, Y. and Li, H., 2017. Seismic data reconstruction with Shearlet transform based on compressed sensing technology. OGP, 52: 220-225.